Astron. Astrophys. 350, 529–540 (1999)

ASTRONOMY AND ASTROPHYSICS

Strong H_2O and high-J CO emission towards the Class 0 protostar L1448-mm⋆

B. Nisini[1,2], M. Benedettini[2], T. Giannini[1,2,3], E. Caux[4], A.M. Di Giorgio[2], R. Liseau[5], D. Lorenzetti[1,2], S. Molinari[6], P. Saraceno[2], H.A. Smith[7], L. Spinoglio[2], and G.J. White[8,5]

[1] Osservatorio Astronomico di Roma, 00040 Monteporzio Catone, Italy
[2] CNR-Istituto di Fisica dello Spazio Interplanetario, Area di Ricerca Tor Vergata, Via Fosso del Cavaliere, 00133 Roma, Italy
[3] Istituto Astronomico, Università La Sapienza, Via Lancisi, 29 00161 Roma, Italy
[4] CESR, B.P.4346, 31028 Toulouse Cedex 04, France
[5] Stockholm Observatory, 133 36 Saltsjöbaden, Sweden
[6] Infrared Processing and Analysis Center, Pasadena, CA 91125, USA
[7] Harvard – Smithsonian Center for Astrophysics, 60 Garden Street, Cambridge, MA, USA
[8] Physics Department, Queen Mary and Westfield College, University of London, Mile End Road – London E1 4NS, UK

Received 25 January 1999 / Accepted 22 July 1999

Abstract. The spectrum of the Class 0 source L1448-mm has been measured over the wavelength range extending from 6 to 190 μm with the Long Wavelength Spectrometer (LWS) and the Short Wavelength Spectrometer (SWS) on the Infrared Space Observatory (ISO). The far infrared spectrum is dominated by strong emission from gaseous H_2O and from CO transitions with rotational quantum numbers $J \geq 14$; in addition, the H_2 pure rotational lines S(3), S(4) and S(5), the OH fundamental line at 119 μm, as well as emission from [O I] 63 μm and [C II] 158 μm are also observed. The strong CO and water emission can be consistently explained as originating in a warm gas component at $T\sim$700–1400 K and $n_{\rm H_2}\sim$(3–50) 10^4 cm^{-3}, which fills about 0.2–2% of the $\sim$75″ LWS field of view (corresponding, assuming a single emitting region, to a physical size of about (3–12)″ or (0.5–2) 10^{-2} pc at d = 300 pc). We derive an H_2O/CO abundance ratio $\sim$5, which, assuming a standard CO/H_2 abundance of 10^{-4}, corresponds to H_2O/H_2 $\sim 5\,10^{-4}$. This value implies that water is enhanced by about a factor $\sim 10^3$ with respect to its expected abundance in the ambient gas. This is consistent with models of warm shocked regions which predict that most of the free atomic oxygen will be rapidly converted into water once the temperature of the post-shocked gas exceeds $\sim$ 300 K. The relatively high density and compact size inferred for this emission may suggest an origin in the shocked region along the molecular jet traced by SiO and EHV CO millimeter line emission. Further support is given by the fact that the observed enhancement in H_2O can be explained by shock conditions similar to those expected to produce the abundant SiO observed in the region. L1448-mm shows the largest water abundance so far observed by ISO amongst young sources displaying outflow activity; we argue that the occurrence of multiple shocks over a relatively short interval of time, like that evidenced in the surroundings of L1448-mm, could have contributed to enrich the molecular jet with a high H_2O column density.

Key words: stars: formation – stars: individual: L1448-mm – ISM: jets and outflows – ISM: molecules – infrared: ISM: lines and bands

1. Introduction

The Class 0 source L1448-mm (also called L1448C) is a deeply embedded, young low mass protostellar object ($L \sim 10\,L_\odot$) located in the core of the L1448 dense cloud (at a distance d = 300 pc, Cernis 1990). It emits strongly at millimeter and centimeter wavelengths, while the IRAS satellite was only able to detect weak far infrared emission (Curiel et al. 1990; Bachiller et al. 1991a; Barsony et al. 1998). H_2O maser emission has also been detected from this source, with an intensity which is significantly higher than that usually observed in young sources of similar luminosity (Chernin 1995). This source drives a young and highly collimated bipolar outflow (Bachiller et al. 1990) which has been mapped by means of different molecular tracers. These observations reveal a complex structure where components with different physical properties co-exist and probably are interacting together. CO J=2→1 and 1→0 observations, in particular, have revealed that in addition to the high velocity gas which outline the overall outflow structure, there are several spatially and spectrally separated clumps, aligned with the outflow axis, which have extreme velocities up to 70 km s^{-1} and sizes of $\sim$ 0.03 pc (the so-called "molecular bullets", Bachiller et al. 1990). These clumps lie in pairs located symmetrically with respect to the mm source and have similar but opposite velocities. This has lead to the suggestion that these bullets are

Send offprint requests to: Brunella Nisini
(bruni@coma.mporzio.astro.it)

⋆ Based on observations with ISO, an ESA project with instruments funded by ESA Member States (especially the PI countries: France, Germany, the Netherlands and the United Kingdom) with the participation of ISAS and NASA

produced by successive ejections from the central source. In addition, their alignment along the outflow axis al so suggests that they trace the jet which entrains the ambient molecular material in a biconical cavity, which is observed through lower velocity gas (Bachiller et al. 1995). SiO emission has also been observed associated with these clumps, with an abundance enhancement of 10^4–10^5 times greater than typical values of quiescent molecular clouds (Bachiller et al. 1991b; Guilloteau et al. 1992; Dutrey et al. 1997). Such high SiO abundance could be generated by shocks with velocities greater than 25 km s^{-1}, that are capable of removing silicon from dust grains (Schilke et al. 1997). High angular resolution images in SiO J=2→1 close to the mm source (Guilloteau et al. 1992) show that this emission is distributed along a jet-like structure, where it is possible to define different sub-clumps of size $\sim 4''$, whose kinematical timescales are $\sim$ 100 yr.

The outflow from L1448 has also been mapped extensively in H_2 emission (e.g. Bally et al. 1993; Davis et al. 1994; Davis & Smith 1995). The strongest H_2 features are seen in the blue lobe of the outflow, with an arc-like structure which surrounds the high velocity molecular jet. H_2 emission is also observed at the end of the redshifted lobe, but is not detected from the innermost molecular clumps which lie close to the mm source, presumably due to higher exctinction in this region.

The observational scenario outlined above shows that along the L1448 outflow and in particular in the environment close to the mm source, different excitation regimes are probed by the different molecular lines; in particular, low velocity CO traces relatively low density gas at $T_{\rm ex}\sim$10–30 K, the CO and SiO emission in the molecular clumps indicates higher densities (10^5–10^6 cm^{-3}) and temperatures of about one hundred K, and finally the H_2 emission traces material at temperatures in excess of 2000 K. It is therefore clear that there is an observational gap in our ability to trace gas with excitation temperatures between 100 and 2000 K; this is because the gas cooling in this temperature regime occurs mainly through the emission of atomic and molecular lines like [O I], H_2O, high-J CO, OH and H_2 transitions, which all fall in the mid to far infrared spectral range, which is not accessible from the ground. Observations with the Infrared Space Observatory (ISO, Kessler et al. 1996) allow this gap to be filled, giving for the first time the opportunity to spectroscopically investigate the entire spectral range from 3 to 200 μm. Spectra obtained with ISO towards a number of young sources driving molecular outflows have already shown that the circumstellar gas in such sources is cooled mainly by line emission from O^0 and CO (Nisini et al. 1999; Nisini et al. 1998; Saraceno et al. 1998). Emission from gas phase H_2O has been observed in some sources (e.g. Saraceno et al. 1998), but even if the derived abundance has been found higher than the expected interstellar value in quiescent clouds (van Dishoeck et al. 1993), its contribution to the gas cooling is never found to be as important as expected in the warm gas around protostars, where the water abundance can be significantly enhanced due to either the evaporation of icy grain mantles or to molecular formation in high temperatures ($\gtrsim$ 300 K) gas-phase chemical reactions. Here we present the first case in which cooling by water dominates over that of any other species which is present in the investigated region.

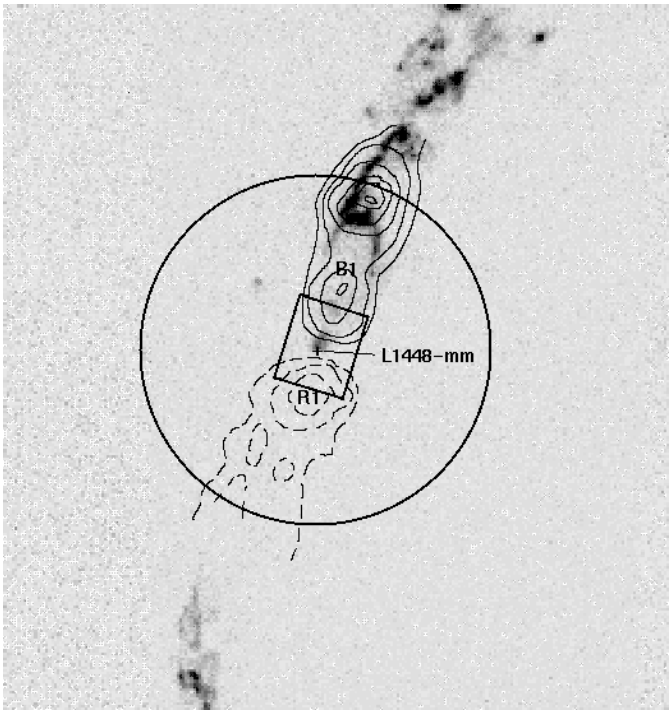

Fig. 1. The LWS and SWS beams of 75″and 14″ ×20″respectively are superimposed on a H_2(1-0)S(1) + continuum emission from Davis and Smith (1995). The contours delineate the EHV CO emission in the blue (solid line) and red (dotted line) lobes of the outflow (adapted from Guilloteau et al. 1992). R1 and B1 indicates the EHV molecular bullets closest to the central source.

2. Observations and results

L1448-mm (α_{1950} = 3$^{\rm h}$ 22$^{\rm m}$ 34$^{\rm s}$.3, δ_{1950} = 30° 33′ 35″) was observed with the LWS (Long Wavelength Spectrometer, Clegg et al. 1996) and SWS (Short Wavelength Spectrometer, de Graauw et al. 1996) on the ISO satellite. In Fig. 1 the apertures of the two instruments are superimposed on a 2.12 μm map of L1448 to show the region covered by the observations.

2.1. LWS observations

A low resolution (R $\sim$ 300) spectrum of the source extending from 45 to 197 μm was obtained with the LWS during revolution 653 (August 30, 1997). The spectrum was oversampled by a factor of four and each spectral sample had 10 s integration, for a total integration time of 4265 s. The raw data were reduced and calibrated using version 7 of the LWS pipeline, which resulted in an absolute intensity calibration within 30% (Swinyard et al. 1996). Post-pipeline processing included the removal of spurious signals resulting from cosmic ray impacts, and averaging of the various grating scans from each detector. The line fluxes, obtained from gaussian fitting to the spectral profiles, are listed in Table 1, where the associated errors refer to the rms noise of the local baseline. We show in Fig. 2 the global spectrum obtained

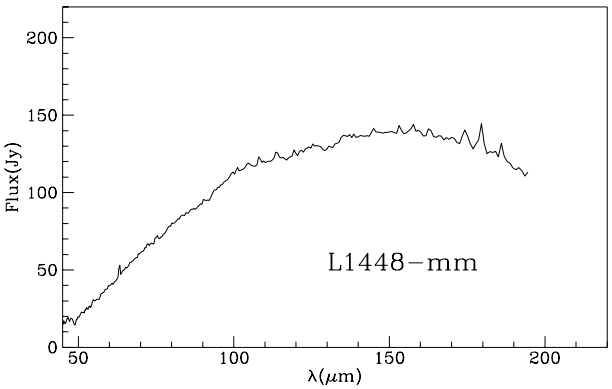

Fig. 2. The LWS spectrum of L1448-mm obtained by matching each other the ten LWS detectors and rebinning the data at the instrumental resolution

by merging together the sub-spectra obtained from the ten LWS detectors just to give an idea of the relative contribution of the line emission with respect to the underline continuum, while a detailed account for the FIR continuum emission of the mm source will be given elsewhere (Nisini et al. 1999, Paper II).

Fig. 3 shows the continuum subtracted (by second order polynomial fitting) spectrum from 50 to 190 μm while in Fig. 4 the [O I] 63μm line is plotted. The spectrum appears extremely rich in rotational lines of both carbon monoxide and water vapour. All the CO transitions with J from 14 (the lowest transition observable with the LWS, at 186 μm) to 21 were detected. The J=22 line is not seen to a 3σ level of 7 10^{-20} W cm^{-2}, but the J=25 line at 104.5 μm is clearly detected with a S/N of about 5. The J=23, 24 and 26 lines are blended with strong H_2O transitions which have a FWHM slightly broader than the instrumental resolution element of 0.6 μm. An attempt to deblend with a two gaussian fit was made for the J=26 and J=24 lines, which are separated from the adjacent p-H_2O 2_{20}-1_{11} and o-H_2O 2_{21}–1_{10} lines by about 0.5 and 0.6 μm. The CO J=23 at 113.46 μm is however too close to the o-H_2O 4_{14}–3_{03} line (at 113.54 μm) to permit a meaningful deblending. The fact that the observed line peaks at 113.65 μm suggests however that most of the flux can be attributed to the water line.

Water lines are observed in both the ortho and para form; almost all the backbone lines up to excitation temperatures of about 500 K are present, plus most of the strongest transitions which fall in the LWS spectral range (see Fig. 6). In addition to CO and water, the OH fundamental at 119 μm (a blend of the four low-lying transitions of the 3/2 ladder) is also observed. An upper limit to the 99 μm line of OH $^2\Pi_{1/2}$ 5/2–3/2 was set by attempting to deblend it from the nearby o-H_2O 5_{05}–4_{14} line at 99.5 μm. The [C II] 158μm and [O I] 63μm lines are the only atomic emission lines present in the spectrum.

2.2. SWS observations

The SWS was used in the AOT SWS02 mode to scan the H_2 pure rotational lines from S(1) to S(7) and the [Si II] 35μm line with a resolution ranging from 1000 to 2000. The beam sizes of these observations (obtained during revolution 814, on February 6, 1998) are 14″×20″ for the lines from S(3) to S(7), 14″×27″ for the S(1), S(2) and 20″×27″ for [Si II].

Each line was integrated for a total time of 200 s. The data were reprocessed through the SWS pipeline version 6; systematic flux errors due to the SWS calibration uncertainties are estimated to be about 30% (Schaeidt et al. 1996). Of the scanned lines, only the H_2 S(3), S(4) and S(5) were detected and their spectrum is shown in Fig. 5. The measured and upper limits fluxes are reported in Table 2.

Table 1. Emission lines measured with LWS toward L1448-mm

λ_{obs} (μm)	Line id.	λ_{vac} (μm)	F (10^{-20} W cm^{-2})	ΔF[a]
63.20	[O I] $^3P_1 \rightarrow {}^3P_2$	63.18	29	1.4
90.06	p-H_2O 3_{22}-2_{11}	89.99	5.1	1.3
98.98	OH $^2\Pi_{1/2}$5/2-3/2	98.7	<4.5	
99.50	o-H_2O 5_{05}-4_{14}	99.49	13.	1.1
100.71	CO 26-25	100.46	3.3	1.1
101.12	p-H_2O 2_{20}-1_{11}	100.98	9.9	1.8
104.46	CO 25-24	104.44	5.7	1.1
108.20	o-H_2O 2_{21}-1_{10}	108.07	13.	1.2
108.84	CO 24-23	108.76	4.2	1.2
113.65	CO 23-22	113.46	15.	2.5
	o-H_2O 4_{14}-3_{03}	113.54		
119.42	OH $^2\Pi_{3/2}$5/2-3/2	119.4	9.1	1.1
121.72	o-H_2O 4_{32}-4_{23}	121.72	4.8	1.5
124.15	CO 21-20	124.19	3.5	0.6
125.54	p-H_2O 4_{04}-3_{13}	125.35	3.8	1.0
130.32	CO 20-19	130.37	4.1	0.8
132.55	o-H_2O 4_{23}-4_{14}	132.41	2.6	0.6
137.12	CO 19-18	137.20	4.8	0.7
138.55	p-H_2O 3_{13}-2_{02}	138.53	3.6	0.6
144.71	CO 18-17	144.78	5.1	0.7
153.26	CO 17-16	153.27	6.1	0.9
157.74	[C II] $^2P_{3/2} \rightarrow {}^2P_{1/2}$	157.74	7.2	0.7
162.83	CO 16-15	162.81	6.1	1.0
173.62	CO 15-14	173.63	8.5	2.0
174.62	o-H_2O 3_{03}-2_{12}	174.63	11.	3.0
179.53	o-H_2O 2_{12}-1_{01}	179.53	22.	3.0
180.56	o-H_2O 2_{21}-2_{12}	180.49	6.0	2.4
185.95	CO 14-13	186.00	9.3	1.4

[a] Errors are statistical and upper limits 3σ

Table 2. Emission lines measured with SWS towards L1448-mm

Line	λ (μm)	F (10^{-20} W cm^{-2})	ΔF[a]
S(7)	5.5112	<9.6	
S(6)	6.1086	<7.5	
S(5)	6.9095	5.9	1.7
S(4)	8.0251	1.6	0.4
S(3)	9.6649	1.3	0.4
S(2)	12.279	<5.7	
S(1)	17.035	<0.8	
[Si II]	34.814	<2.1	

[a] Errors are statistical and upper limits 3σ

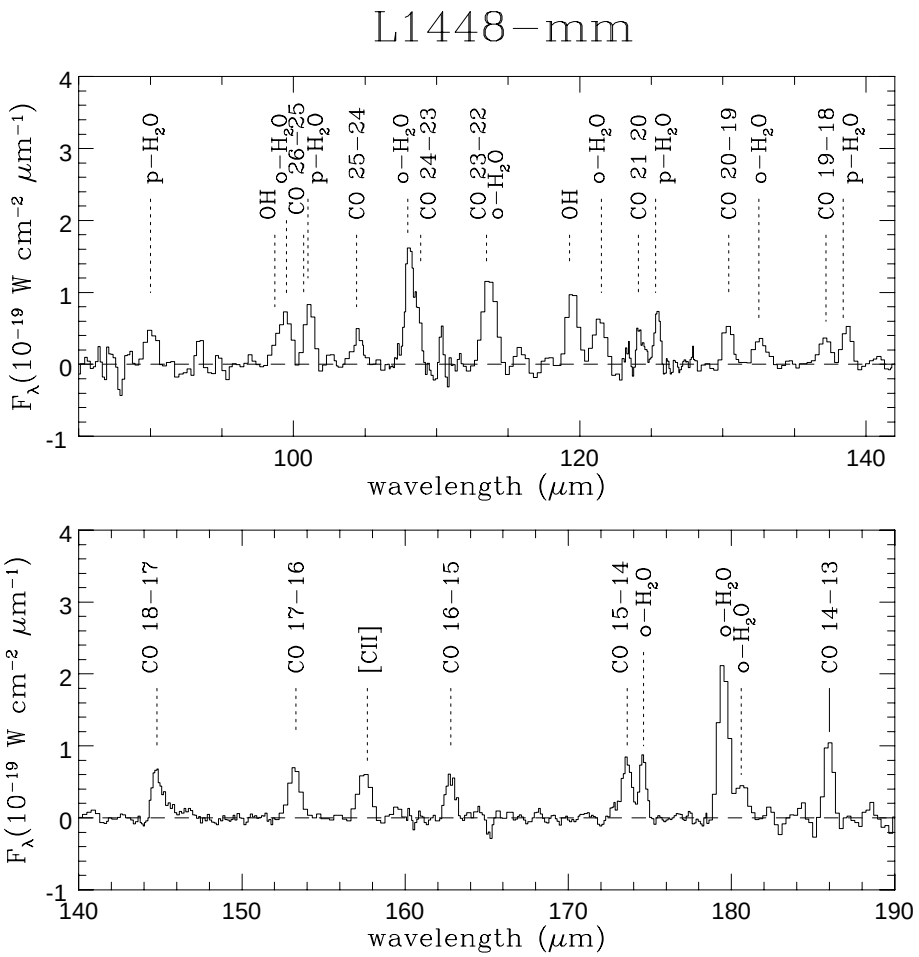

Fig. 3. The continuum subtracted LWS spectrum of L1448-mm in the wavelength range where molecular emission lines have been detected. This part of the spectrum also includes the [C II] 158 μm line.

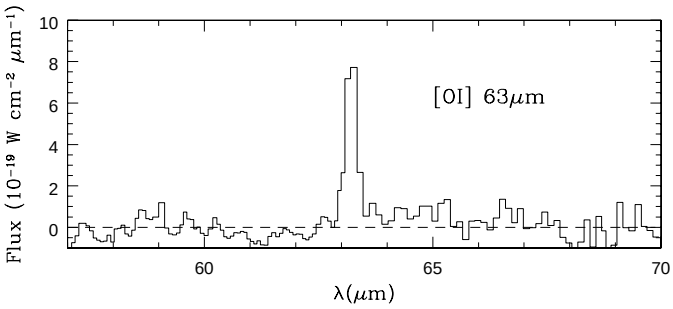

Fig. 4. The continuum subtracted portion of the LWS spectrum showing the [O I] 63 μm line.

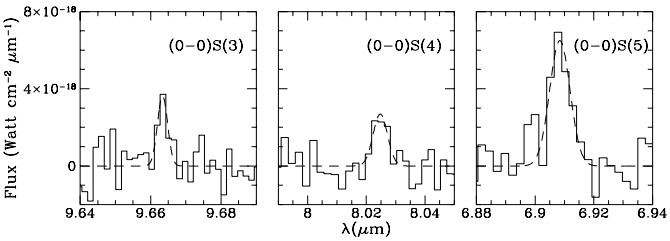

Fig. 5. Continuum subtracted SWS spectra of the H_2 pure rotational lines detected towards L1448-mm. Gaussian fits through the data are indicated by dashed lines.

3. Analysis of molecular emission

To understand the origin of the observed strong molecular emission, we first want to derive the physical parameters, averaged over the rather large LWS beam ($\sim 75''$), which characterises the different gas components. For this purpose, the line emission from CO, H_2O and OH have been analysed by solving the radiative transfer in the line simultaneously with the level populations, under the Large Velocity Gradient (LVG) approximation in a plane-parallel geometry. Given the average nature of the observed emission and the uncertainty on the exact geometry involved, we did not attempt to consider a more realistic geometrical model. In principle, the emission from warm dust could be efficient in the radiative excitation of H_2O and OH; however, the influence of the local radiation field has not been taken into account in the radiation transfer calculations considering that the continuum source has a temperature of about 30 K and a dust opacity of only 0.07 at 200μm (Barsony et al. 1998), while gas temperatures in excess of 500 K are implied by our observed lines (see Fig. 6).

In these approximations, the expected flux of a transition at frequency ν is given by:

$$F_\nu = \frac{\Omega}{4\pi} \int_{\Delta z} h\nu \, A_\nu \, \beta_\nu(\tau_\nu) \, f_u \, n_X \, dz \;\; \mathrm{erg\,s^{-1}\,cm^{-2}}, \qquad (1)$$

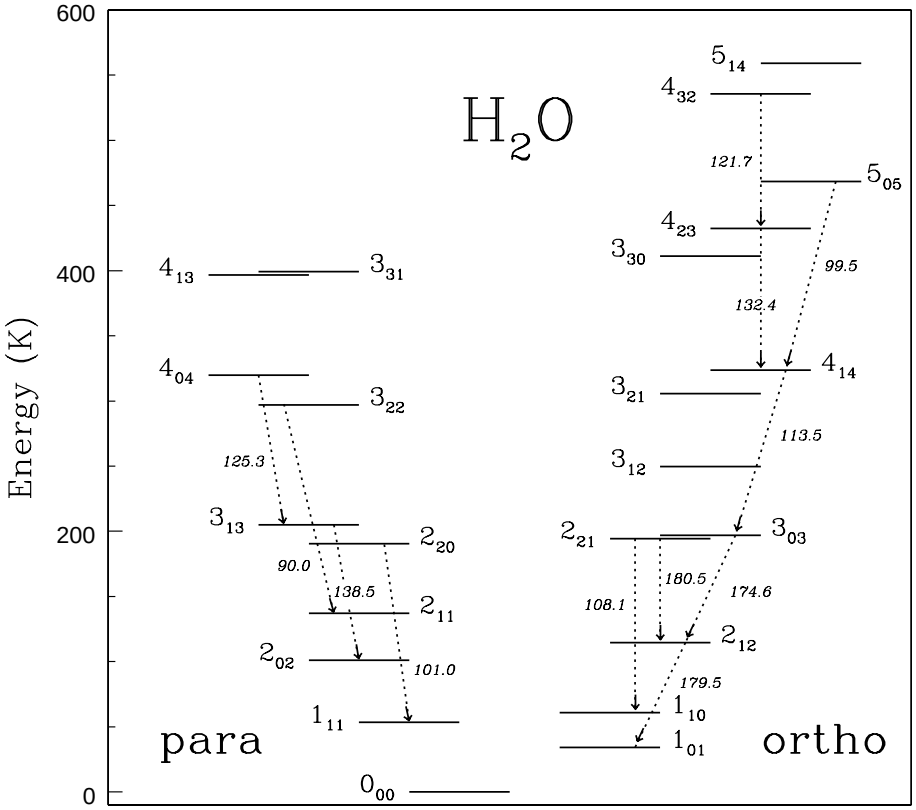

Fig. 6. Energy level diagram of H_2O with the transitions observed by LWS in L1448-mm and their wavelengths in microns indicated.

where A_ν is the spontaneous radiative rate, f_u is the fractional population of the upper level of the transition, n_X is the number density of the considered molecular species, Δz is the depth of the emitting region subtending a solid angle Ω, and β_ν is the angle-averaged escape probability which depends on the line optical depth τ_ν through the relationship (valid for a plane-parallel geometry, Scoville & Solomon 1974):

$$\beta_\nu = \frac{1 - e^{-3\tau_\nu}}{3\tau_\nu}. \quad (2)$$

The optical depth can be expressed as:

$$\tau_\nu = \frac{c^3}{8\pi\nu^3} A_\nu f_u (\frac{n_l g_u}{n_u g_l} - 1) n_X \left| \frac{1}{dV/dz} \right|, \quad (3)$$

where dV/dz is the velocity gradient in the region and n_u, n_l and g_u, g_l are the populations and the statistical weights of the upper and lower levels respectively.

If we assume an homogeneous slab where the total velocity dispersion is ΔV this last expression can also be written:

$$\tau_\nu = \frac{c^3}{8\pi\nu^3} A_\nu f_u (\frac{n_l g_u}{n_u g_l} - 1) \frac{N_{\rm X}}{\Delta V}, \quad (4)$$

making explicit the dependence on the column density ($N_{\rm X}$) of the particular molecule.

The fractional population is given by the equations of the statistical equilibrium which, for a collisionally excited molecule, depend on the local temperature and density as well as on β_ν.

From the above expressions we can see that the line intensity depends on several free parameters (temperature, density, size and depth of the emitting region, velocity dispersion) some of which are related together, and thus difficult to be simultaneously constrained even with the large number of observed lines. However, the high-J CO lines are likely to be optically thin ($\beta_\nu \rightarrow 1$), in which case their relative ratios depend only on the excitation temperatures and densities. In addition, the H_2 lines, being optically thin and thermalised, can further constrain the gas temperature. The temperature and density derived in this way can then be used as fixed parameters in modelling the water and OH lines, which are very sensitive to opacity effects because they have their energy levels connected by strong radiative transitions.

3.1. CO and H_2

The downward collisional rates for CO levels with $J < 60$ and $T > 100$ K were calculated using the γ_{J0} coefficients taken from McKee et al. (1982), while the upward rates were computed using the principle of detailed balance. Radiative decay rates were taken from Chackerian & Tipping (1983). If we look at fluxes of the observed CO lines plotted as a function of the upper level rotational quantum number (Fig. 7), we note that the transitions with J=24, 25 and 26 have flux levels which are too high, compared to the lower transitions, to be excited in the same gas component. We have therefore attempted only to fit the transitions with $J < 21$. From their ratios we derive a temperature ranging from 700 to 1400 K and a density in the range $3\,10^4$ to $5\,10^5$ cm^{-3}. These limits were obtained after considering all the model fits which were compatible with the errors associated

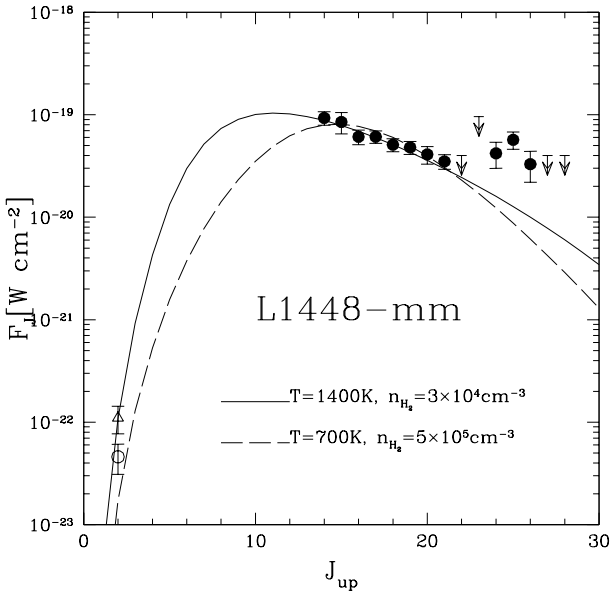

Fig. 7. Model fits through the observed CO lines. The range of temperatures and densities compatible with the observations are indicated. The total flux in the J=2→1 line from Bachiller et al. (1990) is also reported (open triangle) together with the J=2→1 emission relative only to the EHV component (open circle). The higher observed J lines (J=24, 25 and 26) have fluxes too high to be fitted by the same parameters as the other lines, suggesting the presence of a second component.

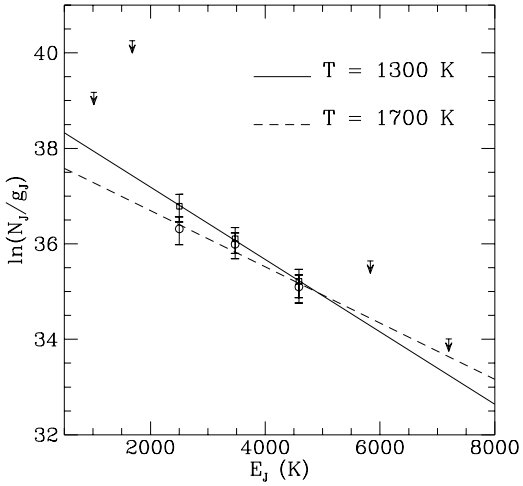

Fig. 8. H_2 excitation diagram. The open circles are the observed line fluxes to which a dereddening of A_V=5 mag has been applied, while open squares are dereddened with A_V=11 mag

with the lines. In Fig. 7 we also report the J=2→1 measurement taken from Bachiller et al. (1990): we see that both the intensity integrated over all velocities (open triangle) and the contribution just of the EHV gas (open circle) lie inside our considered parameter range. In particular, temperatures greater than 1400 K would not agree with the total flux in the J=2→1 line while the 700 K fit already miss the J=2→1 completely; temperatures lower than this value would also fail to reproduce both the lower and higher J lines observed by LWS, giving rise to curves narrower than the observed flux distribution.

Given the high uncertainty on the flux determination of the J=24 and 26 lines due to their blending with the much stronger H_2O lines (see previous section), we have not attempted to fit the second component. However, the fact that it should peak at $J\sim$24, indicates that its temperature cannot be lower than about 2000 K.

The analysis of the H_2 (0–0) lines gives a further way to constrain the gas temperature. Indeed, these lines originate from quadrupole transitions and are therefore optically thin. In addition, they have critical densities lower than 10^4 cm^{-3} [(1)], implying that they are very quickly thermalised; their ratios can therefore be used to directly estimate the gas temperature. This can be better visualised in a rotational diagram (Fig. 8), where the natural logarithm of $N(J)/g(J)$, the column density for a given upper level divided by its statistical weight, is plotted against the excitation energy of the upper level. To construct this diagram, the spontaneous radiative rates were taken from Turner et al. (1977), and an ortho- to para- H_2 equal to 3 was adopted. For a Boltzmann distribution, the slope of this plot is inversely proportional to the kinetic temperature of the gas. We note that the three detected lines were all observed with the same beam size, and therefore no beam filling correction is needed.

The S(3) line at 9.7 μm is particularly sensitive to extinction corrections, lying in the middle of the silicate absorption feature. An average visual extinction of about 5 mag was estimated towards the region covering the entire outflow (Bachiller et al. 1990), but of course the reddening could be much larger than this value on smaller scales, particularly in the surroundings of the mm source. Given the fact that the S(4) and S(5) lines are much less affected by reddening than the S(3) line, we can make a rough estimate of the extinction correction by imposing that the S(3) transition should lie on the same line as the other two transitions in the excitation diagram. In this way we estimate $A_V \sim 11$ mag. Fig. 8 shows the derived excitation temperatures both assuming A_V=5 mag and A_V=11 mag. Given also the uncertainty associated with the measurements, a range of temperatures from 1300 to 1700 K can be deduced. Therefore, in the assumption that the H_2 lines are emitted in the same region as the CO lines, a temperature between 1300 and 1400 K would be favourite as the best estimate to simultaneously reproduce the H_2 and the CO observations. The corresponding density values from the CO fits would in this case range between 3 and 6 10^4 cm^{-3}. However, given the different beam sizes of the LWS and SWS instruments, the possibility that they are actually tracing different gas components cannot be ruled out. We will therefore conservatively assume that CO temperatures as low as 700 K cannot be excluded.

3.2. H_2O and OH

Assuming that the water lines originate in the same region as the CO lines, we can take the temperature and density as derived

[1] this has been checked to be true in the temperature range 100–2000 K by using the collisional rates from Danby et al. (1987)

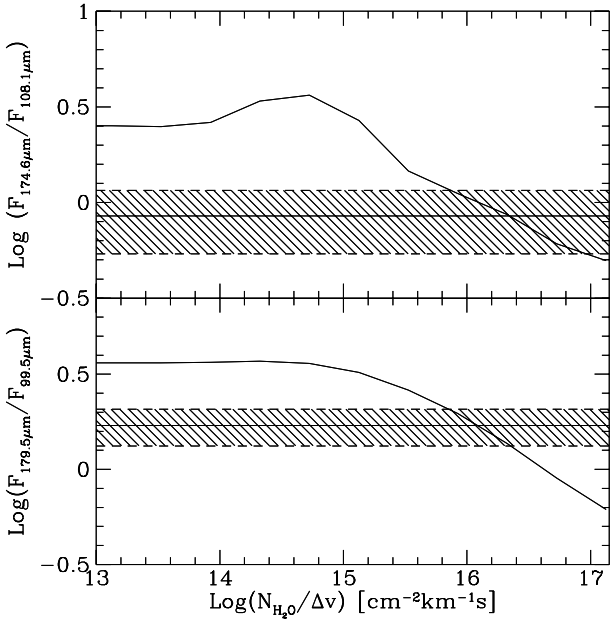

Fig. 9. Ratio of intensities of the 3_{03}–2_{12} 174.6 μm to the 2_{21}–1_{10} 108.1 μm (upper panel) and of the 2_{21}–2_{12} 179.5 μm to the 5_{05}–4_{14} 99.5 μm (lower panel) H_2O lines, as a function of the $N(H_2O)/\Delta V$ parameter for a gas temperature T= 1400 K and a volume density n_{H_2}=3 10^4 cm^{-3}. The straight line indicates the observed value while the dashed region delimits the range of uncertainty.

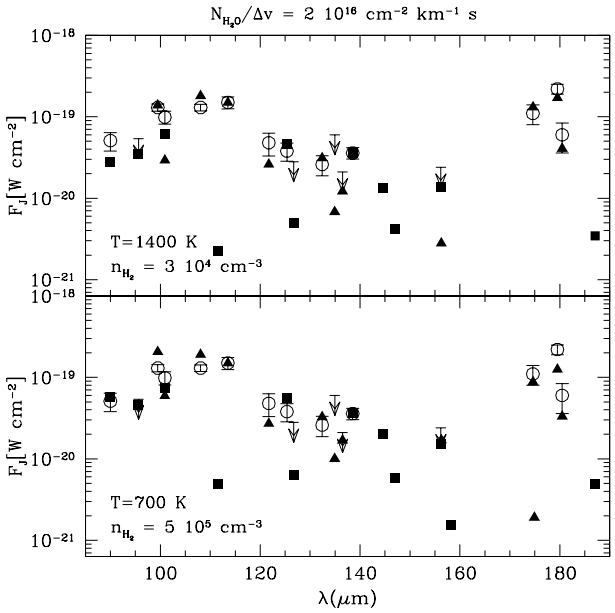

Fig. 10. Comparison of the modelled H_2O line fluxes (triangles and squares indicate the lines in the ortho and para form respectively) with the observations (open circles) in the two extreme conditions derived from the CO fit. We note that the theoretical fluxes for the lines not observed in the LWS spectrum are all below the detectability threshold.

from the CO analysis to model the observed H_2O fluxes. We will in particular consider the two extreme conditions derived from CO, T ∼1400 K and n ∼ 3 10^4 cm^{-3}, and T ∼700 K and n ∼ 5 10^5 cm^{-3}, referring to them as the "high" and "low" temperature cases respectively. The water spectrum has been computed considering 45 levels for both the ortho and para species (i.e. considering the levels up to excitation temperatures of ∼ 2000 K) and adopting radiative rates taken from Chandra et al. (1984) and H_2O-H_2 collisional rates from Green et al. (1993). We assume an ortho/para abundance ratio of 3, equal to the ratio of the statistical weights of their nuclear spins.

Having fixed the temperature and density, we see from Eqs. (1), (2) and (4) that the other parameters affecting the absolute flux intensity of the water lines are the velocity dispersion, the H_2O column density and the projected area of the emitting region. The optical depth in the lines is proportional to $N(H_2O)/\Delta V$ and since the ratios of different lines depend on their relative optical depths through the escape probability (Eqs. [2] and [4]), we can use them to constrain a value of $N(H_2O)/\Delta V$. The dependence of the line ratios on this parameter is shown in Fig. 9 for two different sets of lines. From the figure it appears clear that a unique value of $N(H_2O)/\Delta V$ can be effectively derived from a single ratio providing that the opacity of the considered lines is neither too high ($\tau \to \infty$) so that their absolute intensities approach the blackbody value, nor too low ($\tau \to 0$) that their relative ratios become independent from the column density. The best fit consistent with all the observed ratios gives $N(H_2O)/\Delta V$ = 2 10^{16} cm^{-2} km^{-1} s for either the "high" and "low" temperature cases. A comparison of the observed line fluxes with those predicted by these models is shown in Fig. 10. We see that both cases reproduce quite well the observations, reflecting the difficulty in determining the physical parameters of the emission using the water lines alone; however, the "high" temperature case seems to give a slightly better agreement with the data, especially because it is able to reproduce the observed 179.5 μm line, which is the strongest line observed in the spectrum.

The absolute line intensity depends on both $N(H_2O)$ and Ω, which can be independently derived once a linewidth ΔV is assumed. To estimate ΔV we assume that the observed emission is related to the outflow activity taking place in the close environment of the millimeter source. This has been traced in many different molecular lines (e.g. H_2, CO, SiO), having widths ranging from 20 to 50 km s^{-1}. Taking this range of values we derive a water column density of (0.4–1)10^{18} cm^{-2}; the projected area of the emitting region in the "high" temperature regime is then (50–120) arcsec^2 (i.e. 7–12″ diameter assuming a single emitting region), implying that about 2% of the LWS beam is filled with emitting gas. Adopting this source size, the CO column density can be now estimated from the observed CO line fluxes, giving N(CO)= (0.6–3)10^{17} cm^{-3} (a range which also takes into account the absolute flux calibration errors). We find therefore that the H_2O/CO abundance ratio is ∼5. Hence, for the standard CO abundance of 10^{-4}, the water abundance is ∼ 5 10^{-4}, implying an enhancement with respect to the ambient gas of a factor ∼10^3 (Bergin et al. 1995).

On the other hand, assuming the "low" temperature regime a more compact region of 3–5″ of diameter is derived from the water lines; since however the intrinsic CO line intensity of the

considered transitions is higher than in the "high" temperature case, the implied CO column density is similar in the two cases and consequently the H_2O/CO ratio remains almost unchanged. This makes us confident that the derived value of the water abundance does not depend significantly on specific values adopted for the physical conditions and projected area, the only assumption affecting this value being that CO and water are emitted by the same gas component.

Finally, we also remark that our model predicts a population inversion in the 22 GHz $6_{1,6}$–$5_{2,3}$ transition, which has been detected in the form of strong masering spots aligned with the stellar outflow (Chernin 1995), but we are unable to reproduce the large line luminosity observed; the 22 GHz maser is however localised in dense ($n_{\rm H_2} > 10^6$) and very compact regions probably having the optimal geometry for producing the strong masering, while the LWS observations probe emission on larger scales.

Very high abundances of gas-phase H_2O have so far been estimated only for the Orion region (Harwit et al. 1998) but never in low mass protostars similar to L1448, since the typical values in these sources are of the order of (1–5) 10^{-5} (Liseau et al. 1996; Saraceno et al. 1998; Ceccarelli et al. 1998). In this respect, L1448-mm seems to have an exceptionally high water abundance, indicating that the processes responsible for the production of gas-phase water are particulary efficient here. We will discuss this point further in the next section.

Finally, adopting the same parameters as derived from the above analysis also for OH, from the observed 119 μm flux we deduce a column density N(OH) of (0.7–1.3) 10^{16} cm^{-2} and therefore an X(OH)$\sim 10^{-5}$, i.e. 2 10^{-2} times the water abundance. For the molecular parameters and assumptions in the modelling of the OH, we refer to Giannini et al. (1999).

Table 3 summarises the derived quantities for the observed molecular species.

3.3. The N(H_2) column density

The absolute intensities of the observed H_2 lines can in principle be used to derive the H_2 column density if the beam filling factor is known. Adopting the hypothesis that the high-J CO and H_2 pure rotational line emission is fully enclosed within the relatively smaller SWS beam, we can use the size of the emitting region derived from the above analysis to estimate the $N(H_2)$ of the warm gas, obtaining a value of about 10^{19} cm^{-2}. When compared with the estimated CO column density, this value would imply a CO/H_2 abundance of $\sim 10^{-2}$. This result does not in fact depend on the specific model adopted; a direct measure of the CO/H_2 abundance ratio in the warm gas can be independently given simply by comparing the ratio of two observed lines emitted in the same conditions. Indeed, both the high-J CO and the H_2 lines are optically thin and therefore their ratio is directly proportional to the ratio of their relative column densities. Measuring the ratio for different sets of lines, we always obtain a value of CO/H_2 of the order of 2 10^{-2}. One possible explanation for this anomalous abundance ratio (the interstellar CO/ H_2 abundance is of the order of 10^{-4}, while in dense cores some of the CO can be depleted on grains, further reducing this value, see e.g. van Dishoeck et al. 1993) could be that the region strongly emitting the molecular lines observed by the LWS, has been totally or partially missed by the smaller SWS beam. This in turn would imply, giving the low beam-filling derived for the LWS observations, that the region of emission is not located in the center of the two beams, i.e. coincident with the mm source.

Alternatively, the extinction in the region could be much higer than assumed in our analysis. An A_V value of about 250 mag would be necessary to increase the H_2 S(4) and S(5) observed fluxes by a factor of one hundred, which is needed to find a CO/H_2 abundance ratio similar to the commonly assumed interstellar value. Such a high extinction, which is found only if the observed lines originate from very close to the protostar itself, would strongly affect the (0–0) S(3) line intensity, causing it to deviate too much from the straight line in the rotational diagram. Inconsistencies would be also found with the upper limits of the S(1) and S(2) lines, which, by contrast, are not greatly affected by a large amount of extinction.

A different interpretation could be that in the considered region the hydrogen is not fully molecular but part of it is present in atomic form. This circumstance could happen for instance in protostellar winds, where a significant fraction of atomic hydrogen can be present even if the heavy atoms are processed into molecules (Glassgold et al. 1991). Alternatively, also in the presence of dissociative shocks a significant part of the post-shock gas can be composed of hydrogen which is mainly in atomic form (Hollenbach & McKee 1989). That the flow from young stars can be characterised by an appreciable amount of atomic hydrogen has indeed been demonstrated by the detection of the 21 cm hydrogen line associated with high-velocity molecular outflows (e.g. Lizano et al. 1988).

The different possibilities will be discussed in Sect. 5.

4. O^0 and C^+ emission

C^+ is not usually abundant in shocked regions; dissociative shocks can produce C^+, but its 158 μm emission never exceeds more than $\sim$10% of the [O I] 63 μm emission (Hollenbach & McKee 1989) while our observed [C II] 158 μm /[O I] 63 μm ratio is 0.3. On the other hand, even very weak far UV fields, comparable to the average intertellar field, can produce C^+ fluxes which are detectable with LWS.

Indeed, the flux observed towards L1448-mm, which corresponds to a surface brightness of 4.8 10^{-6} erg s^{-1} cm^{-2} sr^{-1} assuming unit beam filling, is comparable to the value observed at other locations in the cloud (Paper II) and can be accounted for by an average FUV field of only $\sim 4\ G_0$, where G_0 is the FUV flux measured in units of the local interstellar FUV flux (1.6 10^{-3} erg s^{-1} cm^{-2}, Habing 1968). Such a weak field would however be unable to excite the observed [O I] 63 μm emission, which is more likely associated with shock excitation. If we assume that the [O I] 63 μm originates from the same gas which is responsible for the CO, H_2O and OH emission, we derive a column density of O^0 of about 6 10^{16} cm^{-2} (for the given

Table 3. Ranges of physical parameters for the molecular emission

Gas temperature T (K)	700–1400
Gas density $n_{\rm H_2}$ (cm^{-3})	$5\,10^5$–$3\,10^4$
Size ($''$)[a]	3–12
Size (pc)[a]	(0.5–2) 10^{-2}
$N_{\rm CO}$ (cm^{-2})	(0.6–3) 10^{17}
$N_{\rm H_2O}$ (cm^{-2})	(0.4–1) 10^{18}
$N_{\rm OH}$ (cm^{-2})	(0.8–2) 10^{16}
$N_{\rm H_2}$ (cm^{-2})[b]	(0.7–4) 10^{19}
$L_{\rm CO}$ (L$_\odot$)	0.025–0.03
$L_{\rm H_2O}$ (L$_\odot$)	0.045–0.06
$L_{\rm OH}$ (L$_\odot$)	0.005–0.006
$L_{\rm H_2}$ (L$_\odot$)	0.002–0.003

[a] The given range takes into account the lower and upper limits for the emitting region deduced by the different models (see text).
[b] Obtained assuming the same emission area as the other components; see text for a discussion on this point.

conditions, the 63 μm line becomes optically thick at column densities larger than 10^{20} cm^{-2}); this implies an O^0/CO abundance ratio of $\sim$0.3–0.7, and thus an O^0 abundance of $\sim 5\,10^{-5}$, which is about a factor of ten lower than the oxygen interstellar abundance (Meyer et al. 1998). This is indeed what it is expected if a significant fraction of the available oxygen is tied up in H_2O.

5. Discussion

5.1. Excitation mechanisms

In the region we are investigating, which is at the base of the outflow driven by L1448-mm, at least three different excitation regimes are present. In particular CO J=1$\rightarrow$0 and 2$\rightarrow$1 maps show the presence of two different components: a low-velocity outflow ($V \sim 20$ km s^{-1}) having a biconical morphology centered on the mm source, and a much faster moving (projected velocity $\sim$70 km s^{-1}) jet-like emission along the axis of the outflow, which consists of a chain of well defined clumps (molecular "bullets", Bachiller et al. 1990). The LWS beam encompasses only those bullets lying closest to the central source (R1 and B1, symmetrically displaced in the red and blue lobe respectively, see Fig. 1). Such bullets also emit strongly in SiO (Guilloteau et al. 1992), a molecule which is detected only in regions where strong shocks are able to release Si from dust grains into the gas phase, thus allowing the enhancement of the SiO abundance by orders of magnitude (Schilke et al. 1997; Caselli et al. 1997). In addition to millimeter line emission, H_2 1$\rightarrow$0 S(1) emission is also present, with an arc-shaped morphology (knots A and B in Davis & Smith 1995) having the appearance of a bow shock. This region lies at about 30$''$ from the mm source in the blue lobe, and therefore just at the border of the $\sim 75''$ LWS beam and not in the smaller field of view of SWS.

The physical conditions estimated from the LWS spectrum of L1448-mm, can be used to investigate whether the warm gas emission can be associated to any of the above shock environments.We have inferred that the warm component traced by the ISO lines originates from a relatively compact ($\lesssim 12''$) region with temperature less than 1400 K. These characteristics exclude the possibility that the bulk of the observed emission comes from the region outlined by the H_2 knots A and B (at the edge of the LWS beam), which are rather extended and excited at temperatures in excess of 2000 K (Davis & Smith 1995). These knots could however be associated with the second CO emission component at higher temperatures, which is traced by the rotational lines with J>23. We can also exclude that the observed molecular excitation is associated with the low velocity CO, which appears to have a greater spatial extent and smaller column densities than those derived from our analysis. More likely is that the observed molecular emission is associated with the dense molecular bullets: indeed there are several pieces of evidence in favour of this hypothesis. Firstly, the spatial extent of the molecular bullets closest to L1448-mm is about $<2\times15$ arcsec^2 each (Guilloteau et al. 1992), consistent with our derived emission area if we reasonably assume that both the redshifted and blueshifted bullets contribute to the emission. Moreover, the detection of abundant SiO clearly indicates the presence of a shock propagating with $V_{\rm s} > 25$ km s^{-1}, i.e. a shock fast enough to remove the silicon from the dust grains (Schilke et al. 1997): these are the same conditions needed to produce water, since the endothermic reactions for its production become efficient at $T \gtrsim$ 300–400 K, corresponding to shocks with $V > 15$ km s^{-1}.This interpretation is corroborated by the fact that the high-J CO emission lines observed in other low mass young sources have been successfully explained in terms of high-density gas in the presence of compact shocks with velocities from 10 to 25 km s^{-1}(Nisini et al. 1998), indicating that such regions are often associated with outflows, even if they are not necessarily observed at millimeter wavelengths in the form of molecular bullets.

We also consider the possibility that the large water abundance is formed in the original protostellar jet (Glassgold et al. 1991). In favour of this possibility there is the evidence that a large part of hydrogen can be in atomic form, as shown by the high observed value of the CO/H_2 abundance ratio: in addition, the strong water maser spots are aligned with the molecular jet and lie at distances of only 30 AU on each side of the central source, suggesting that they may originate directly from the protostellar jet (Chernin 1995). We note however that under such an hypothesis the emitting region, being located very close to the protostellar source, is fully sampled by both the SWS and the LWS beams, and is best fitted with $T \sim 1400$ K and $n_{\rm H_2} \sim 3\,10^4$ cm^{-3}. Such a low density is comparable to that of the dense core within which L1448-mm is embedded, and it is unlikely to be found in the innermost regions in the envelope of the protostar, where densities in excess of 10^6 cm^{-3} are expected.

5.2. Comparison with shock models

The complex shock structure with multiple excitation regimes present in the surroundings of L1448-mm renders difficult any detailed comparison with simple shock models. Moreover, a further complication is that the presence of episodic phenomena

with timescales as short as few hundred years, would require specific time-dependent modelling. It is however instructive to see to what extent the existing models are able to reproduce the spatial and time averaged physical quantities estimated from the ISO data.

In the previous section it was shown that the observed molecular emission is likely to be associated with the dense molecular jet traced by means of EHV CO and SiO emission. The velocity of such a jet, corrected for the outflow inclination, is about 200 km s^{-1}(Bachiller et al. 1995); the leading shock due to such a high velocity jet would be strongly dissociative. Molecules can be copiously formed behind fast dissociative shocks, once the gas temperature has dropped sufficently to allow H_2 to reform (Hollenbach & McKee 1989; Neufeld & Dalgarno 1989). Although hydrogen becomes completely molecular at temperatures of only few hundred degrees, H_2 starts already to be formed for T $\sim$ 4000 K, rapidly followed by the reactions which bring to the formation of OH, H_2O and SiO:

$$\mathrm{O + H_2 \rightarrow OH + H}$$
$$\mathrm{OH + H_2 \rightarrow H_2O + H}$$
$$\mathrm{OH + Si \rightarrow SiO + H}$$

Our derived temperature range, together with the evidence that the hydrogen may be still partially in atomic form, as testified by the derived high CO/H_2 abundance ratio, are compatible with the above scenario. There are however a number of difficulties to reconcile the derived gas coolings with the fast dissociative shock models. First of all the emission from atomic components like [O I] and [Si II] is too weak. In particular, in fast shock models with pre-shock densities implied by our observations, i.e. $<10^5$ cm^{-3}, cooling due to O^0 is never predicted to be less than that of water, as we in fact see in our case where $L(H_2O)/L(O)$ is 4.5. In addition the [Si II] 35μm line should be only a factor two or three weaker than the [O I] 63μm emission, while our observed upper limit implies a ratio 35μm/63μm which is < 0.07. More important, we note that neither the model by Hollenbach & McKee (1989) nor that by Neufeld & Dalgarno (1989) predict that the production of water behind the dissociative shock can bring the water cooling to exceed the contribution not only of [O I] but also of CO, unless we consider a very dense shock, with pre-shock density $\sim 10^6$ cm^{-3}. Moreover, the presence of highly abundant atomic hydrogen favours a very rapid destruction of gas-phase H_2O through the reaction $H_2O + H \rightarrow OH + H_2$.

The observed high abundance of water molecules is predicted only by low velocity shocks influenced by the presence of a magnetic field; in this circumstance, if the shock velocity is lower than the Alfvén velocity of the ions, a continuos shock, or C-shock, is created, where the temperature across the shock structure changes continuously and never rises above $\sim$ 3000 K, thus preventing the molecular dissociation (Draine 1980). In this stuation, and if the shock velocity exceeds $\sim$ 15 km s^{-1}, water is rapidly formed from the reactions indicated above reaching abundances greater than 10^{-4} (Kaufman & Neufeld 1996). To reconcile the possibility of the presence of a slow shock with the observation of gas velocities travelling at hundreds of km s^{-1}, we could suppose that the gas is travelling into a medium which has already set into motion by the passage of a previous shock; in this case the actual shock velocity ($V_{\rm jet}$–$V_{\rm amb}$) may be significantly lower. Alternatively, the slower shock could be produced by jet components which impact obliquely onto the ambient medium.

If we compare the parameters listed in Table 3 with the predictions of a simple planar and static C-shock model like that of Kaufman & Neufeld (1996), we firstly notice that a temperature range 700–1400 K is consistent with a shock velocity of $\sim$ 15–25 km s^{-1}. For pre-shock densities $\gtrsim 10^4$ cm^{-3} (implied by our estimated post-shock density of $\gtrsim 10^5$ cm^{-3}), the model predicts the following cooling ratios: $L(H_2O)/L(CO) \sim$ 2–3, $L(OH)/L(CO) \sim$ 0.02–0.05 and $L(H_2)/L(CO) \sim$2–3, which can be compared with the observed values of about 2, 0.2, and 0.1 respectively. Cooling by water is therefore substantially in agreement with that predicted. The fact that the H_2 luminosity is significatively lower than the predicted values is indicative that with the SWS we are observing much less H_2 than expected, which strenghtens the hypothesis that the small SWS beam has missed most of the emission region observed by the LWS, as already proposed in Sect. 3.3 to justify the anomalous CO/H_2 ratio. This could happen if, for example, the putative shock lies just at the edge of the molecular bullets rather than all along their lengths, as can be also visualised in Fig. 1. More significant is the greater amount of cooling deduced for the OH with respect to the model. However, the fact that the OH abundance has been estimated from only one line may introduce large uncertainties in the derived value which should therefore be taken with caution.

Specific C-shock models which take into account the Si chemical network and which are able to reproduce the SiO profiles observed in L1448 (Schilke et al. 1997) also predict that the water abundance should be as high as measured by us, although the SiO emission is better explained by a shock with densities of about 10^6 cm^{-3}, i.e. slightly larger than those estimated from the present analysis.

More realistic models for the investigated regions are those which take into account a curvature and therefore a gradient in the excitation conditions along the shocked region ("bow" shock models). In particular, Smith (1991, 1994) considers both non dissociative J and C-type bow shocks; generally speaking our derived temperature and density, and the relative cooling of the various molecules, can be accounted for by these models but any specific constraints on the shock characteristics and geometry would require a more detailed comparison than we are able to make at the present time.

5.3. Comparison with other outflow driving sources

ISO has allowed us to observe, for the first time, the FIR molecular cooling of several shocked regions associated with outflows in young stellar objects (Nisini et al. 1998; Saraceno et al. 1998). In particular, water emission has only been observed in a few sources and always with abundances of the order of 1–5 10^{-5} (e.g. HH54, Liseau et al. 1996; IRAS16293-2422, Ceccarelli et al. 1998; IC1396-N, Molinari et al. 1998; HH25MM, Benedet-

tini et al. 1998). The notable exception to this is the Orion core, where a water abundance of $5\,10^{-4}$ has been found by Harwit et al. (1998) (although Cernicharo et al. (1997) derive for the same region a value X(H_2O)$\sim 10^{-5}$). The interesting aspect is that, although the abundances are fairly constant, the shock conditions inferred for the various sources are rather different; in particular in HH54 and HH25MM gas temperatures of $\sim$ 300–400 K are estimated, indicating shocks propagating with velocities not exceeding ~ 10 km s^{-1}, while IRAS16293 and IC1396-N seem to have significantly higher temperatures, of about 1500 K. For these two sources, therefore, one would expect abundances as high as we observe in L1448-mm, since the shock conditions are very similar. Explanations for a lower water abundance than expected (with respect to shock models) in these sources have been proposed in Ceccarelli et al. (1998) and Saraceno et al. (1998) and include the hypothesis that most of the oxygen is locked into grains, thus rendering inefficient those endothermic reactions which bring all the available gas-phase oxygen into water, or that the time scale required for this process exceeds the dynamical time scale of the outflow. This last hypothesis is not supported by the L1448-mm observations: the dynamical timescale of the L1448-mm outflow has been originally estimated to be as short as 3500 years (Bachiller et al. 1990). Recently, Barsony et al. (1998) revised this value upwords to 32 000 years, which is still very similar to the age of other Class 0 sources, thus not explaining the apparent overproduction of water in terms of a longer available time for its formation. Beside that, we also remark that, for gas temperatures greater than 400 K, the timescale for the H_2O production from gas-phase chemistry is less than 10^3 years (Bergin et al. 1998).

On the other hand the time scales of the individual clumps along the L1448 flow are of the order of 100 years, i.e. much shorter than the total dynamical time. It could be therefore argued that an opposite mechanism would lead to a decrease of the water abundance in older outflows; if the H_2O lifetime is short, the H_2O initially formed could be rapidly lost from the gas-phase either through depletion onto grains and through its conversion into OH. Time-dependent chemical models (Bergin et al. 1998) have shown that, if we consider only the gas-phase chemistry, the shock cooling time is much shorter than the time needed for the gas to return to its pre-shock chemical composition, this latter being in excess of 10^5 years. If however gas-grain interactions are also included, such a time would be shorter for densities $n_{\rm H_2} > 10^4$ cm^{-3} due to a rapid depletion of water onto dust grains. In L1448-mm, the occurrence of multiple shocks over a relatively short interval of time could have conspired to mantain a high water abundance. Indeed, the most recent shock episode is currently propagating into a medium which, having been pre-processed by an earlier shock, has already developed an enhanced water abundance. Specific comparisons with time dependent models of low-velocity shocks would need to be made to understand the influence on the relative cooling ability of the various molecular species over the lifetime of the outflow.

6. Conclusions

The main conclusions of this work can be summarised as follows:

- We have observed the Class 0 source L1448-mm with ISO-LWS and SWS, detecting a far infrared spectrum which is very rich in emission lines from water vapour and CO with rotational number $J \geq 14$. Several other molecular lines were observed including the pure rotational transitions of H_2 from S(3) to S(5) and the OH fundamental line at 119 μm.
- All of the molecular species present in the LWS spectrum can be modelled as being excited in a warm region with T $\sim$700–1400 K and $n_{\rm H_2}$ $\sim 3\,10^4$–$5\,10^5$ cm^{-3}, extending about 0.01 pc. In the hypothesis that the H_2 and CO rotational lines co-exist, a CO/H_2 ratio equal to $\sim 10^{-2}$ is found; such a high value may indicate either that the CO and H_2 emission probe different clumps of gas, or that most of the hydrogen in the region is present in atomic form.
- Applying a LVG model we were able to derive the abundances and the total cooling of all the observed species; the main result from this work is that H_2O is the main coolant of the gas surrounding L1448-mm, with an abundance X(H_2O) of about $5\,10^{-4}$.
- A non-dissociative shock travelling at $V\sim$15–25 km s^{-1} seems to be the most likely excitation mechanism for reproducing most of the characteristics of the emission derived from the ISO spectra. Other alternatives, such as the possibility that the emission is associated with high velocity J-type shocks or it is directly originated in the protostellar envelope have been also considered but seem less compelling in explaining our observations. We suggest that such a low velocity shock originates in a region along the molecular jet traced by SiO and EHV CO millimeter line emission.
- We also speculate that the occurrence of multiple shocks over a relatively short interval of time could explain the very high water abundance observed in L1448, in comparison with other similar protostellar sources.

Acknowledgements. We wish to thank Paola Caselli for useful discussions on shock chemistry and an anonymous referee for her/his valuable comments. We are also grateful to Chris Davis for having provided us with his H_2 2.12 μm figure.

References

Bachiller R., Chernicharo J., Martín-Pintado J., Tafalla M., Lazareff B., 1990, A&A 231, 174
Bachiller R., André P., Cabrit S., 1991a, A&A 241, L43
Bachiller R., Martín-Pintado J., Fuente A., 1991b, A&A 243, L21
Bachiller R., Guilloteau S., Dutrey A., Planesas P., Martín-Pintado J., 1995, A&A 299, 857
Bally J., Lada E.A., Lane A.P., 1993, ApJ 418, 322
Benedettini M., Giannini T., Nisini B., et al., 1998, Proc. of: The Universe as seen by ISO. Paris, 20–23 October 1998, in press
Barsony M., Ward-Thompson D., André P., O'Linger J., 1998, ApJ 509, 733
Bergin E.A., Langer W.D., Goldsmith P.F., 1995, ApJ 441, 222

Bergin E.A., Melnick G.J., Neufeld D.A., 1998, ApJ 499, 777
Caselli P., Hartquist T.V., Havnes O., 1997, A&A 322, 296
Ceccarelli C., Caux E., White G.J., et al., 1998, A&A 331, L17
Cernicharo J., González-Alfonso E., Lefloch B., 1997, In: ISO to the Peak. ISO workshop on analytical spectroscopy, 6–8 October 1997, Madrid
Cernis K., 1990, Ap&SS 166, 315
Chackerian C., Tipping R.H., 1983, J. of Molecular Spectroscopy 99, 431
Chandra S., Varshalovich D.A., Kegel W.H., 1984, A&AS 55, 51
Chernin L.M., 1995, ApJ 440, L97
Clegg P.E., Ade P.A.R., Armand C., et al., 1996, A&A 315, L38
Curiel S., Raymond J.C., Rodriguez L.F., Cantó J., Moran J.M., 1990, ApJ 365, L85
Danby G., Flower D.R., Monteiro T.S., 1987, MNRAS 226, 739
Davis C.J., Dent W.R.F., Matthews H.E., Aspin C., Lightfoot J.F., 1994, MNRAS 266, 933
Davis C.J., Smith M., 1995, ApJ 443, L41
de Graauw T., Haser L.N., Beintema D.A., et al., 1996, A&A 315, L49
Draine B.T., 1980, ApJ 241, 1021
Dutrey A., Guilloteau S., Bachiller R., 1997, A&A 325, 758
Giannini T., Lorenzetti D., Tommasi E., et al., 1999, A&A 346, 617
Green S., Maluendes S., McLean A.D., 1993, ApJ 85, 181
Guilloteau S., Bachiller R., Fuente A., Lucas R., 1992, A&A 265, L49
Glassgold A.E., Mamon G.A., Huggins P.J., 1991, ApJ 373, 254
Habing H.J., 1968, Bull. Astr. Inst. Netherlands 19, 421
Harwit M., Neufeld D.A., Melnick G.J., Kaufman M.J., 1998, ApJ 497, L105
Hollenbach D., McKee C.F., 1989, ApJ 342, 306
Kaufman M.J., Neufeld D.A., 1996, ApJ 456, 250
Kessler M.F., Steinz J.A., Anderegg M.E., et al., 1996, A&A 315, L27
Liseau R., Ceccarelli C., Larsson B., et al., 1996, A&A 315, L181
Lizano S., Heiles C., Rodriguez L.F., et al., 1988, ApJ 328, 763
McKee C.F., Storey J.W.V., Watson D.M., Green S. 1982, ApJ 259, 647
Meyer D.M., Jura M., Cardelli J.A., 1998, ApJ 493, 222
Molinari S., Giannini T., Nisini B., et al., 1998, In: Yun J.L., Liseau R. (eds.) Star Formation with the Infrared Space Observatory. ASP Conference Series vol. 132, p. 390
Neufeld D.A., Dalgarno A., 1989, ApJ 340, 869
Nisini B., Giannini T., Molinari S., et al., 1998, In: Yun J.L., Liseau R. (eds.) Star Formation with the Infrared Space Observatory. ASP Conference Series vol. 132, p. 256
Nisini B., Benedettini M., Giannini T., et al., 1999, A&A 343, 266
Saraceno P., Nisini B., Benedettini M., et al., 1998, In: Yun J.L., Liseau R. (eds.) Star Formation with the Infrared Space Observatory. ASP Conference Series vol. 132, p. 233
Schaeidt S.G., Morris P.W., Salama A., et al., 1996, A&A 265, L55
Schilke P., Walmsley C.M., Pineau des Forêts G., Flower D.R., 1997, A&A 321, 293
Scoville N.Z., Solomon P.M., 1974, ApJ 187, L67
Smith M.D., 1991, MNRAS 253,175
Smith M.D., 1994, MNRAS 266,238
Swinyard B.M., Clegg P.E., Ade P.A.R., et al., 1996, A&A 315, L43
Turner J., Kirby-Docken K., Dalgarno A., 1977, ApJS 35, 281
van Dishoeck E.F., Blake G.A., Draine B.T., Lunine J.I., 1993, In: Levy E.H., Lunine (eds.) Protostars and Planets III. Univ. Arizona Press, Tucson, p. 163